Separation Science and Technology
Publication details, including instructions for authors and subscription information:
http://www.informaworld.com/smpp/title~content=t713708471

Iron-Functionalized Membranes for Nanoparticle Synthesis and Reactions

Scott Lewis[a]; Vasile Smuleac[a]; Alex Montague[a]; Leonidas Bachas[b]; Dibakar Bhattacharyya[a]
[a] Department of Chemical and Materials Engineering, University of Kentucky, Lexington, KY, USA [b] Department of Chemistry, University of Kentucky, Lexington, KY, USA

To cite this Article Lewis, Scott , Smuleac, Vasile , Montague, Alex , Bachas, Leonidas and Bhattacharyya, Dibakar(2009) 'Iron-Functionalized Membranes for Nanoparticle Synthesis and Reactions', Separation Science and Technology, 44: 14, 3289 — 3311
To link to this Article: DOI: 10.1080/01496390903212805
URL: http://dx.doi.org/10.1080/01496390903212805

Separation Science and Technology, 44: 3289–3311, 2009

ISSN: 0149-6395 print/1520-5754 online
DOI: 10.1080/01496390903212805

Taylor & Francis
Taylor & Francis Group

Iron-Functionalized Membranes for Nanoparticle Synthesis and Reactions

Scott Lewis,[1] Vasile Smuleac,[1] Alex Montague,[1] Leonidas Bachas,[2] and Dibakar Bhattacharyya[1]
[1]Department of Chemical and Materials Engineering, University of Kentucky, Lexington, KY, USA
[2]Department of Chemistry, University of Kentucky, Lexington, KY, USA

Abstract: Membrane-based separation processes have been used extensively for drinking water purification, wastewater treatment, and numerous other applications. More recent developments in membrane functionalization have made the use of membrane science important in diverse fields, from tunable separations to catalysis. The focus of this work is to create a common membrane platform for the incorporation of technologies capable of degrading target pollutants. Functionalized membranes capable of metal capture were created using water-based and solvent-based acrylic acid polymerization to synthesize poly (acrylic acid) (PAA) within poly(vinylidene fluoride) (PVDF) membrane pores. The COO^- groups of PAA were used to capture Fe(II), which was then either reduced and doped with Pd to form Fe/Pd nanoparticles or used as-is for free radical generation with hydrogen peroxide. Fe/Pd nanoparticles were synthesized within the pores of a PAA/PVDF membrane functionalized via aqueous (green) chemistry and used to dechlorinate trichloroethylene (TCE) and 2,2′-dichlorobiphenyl (DiCB). A PAA/PVDF membrane containing immobilized Fe(III) was used to obtain controlled free radical generation and target organic (pentachlorophenol) degradation within the membrane pore under convective flow conditions.

Keywords: Dechlorination, Fe/Pd nanoparticles, free radical, PCB, TCE

Received 7 December 2008; accepted 8 May 2009.
Address correspondence to Dibakar Bhattacharyya, Alumni Professor, Department of Chemical and Materials Engineering, University of Kentucky, Lexington, KY 40506, USA. Tel.: (859) 257-2794; Fax: (859) 323-1929. E-mail: db@engr.uky.edu

INTRODUCTION

The field of membrane separation is in a state of a tremendous growth and innovation. Membranes are essential for applications ranging from drinking water purification and wastewater treatment to pharmaceuticals production, food and beverage processing, medical devices, and separations needed for manufacturing chemicals, electronics, and a variety of other products (1–4). New processes are being reported frequently, and existing processes are also being constantly improved in order to enhance their competitiveness (5–7).

Conventional membranes are considered to be a separation media based solely on size (MF, UF), charge and/or size (NF), or solubility (RO, PV)) of species. However, with the advancement of functionalization chemistry and the availability of novel materials, further versatility can be obtained in the form of functionalized membranes. Functionalized membranes can be tailor-made to impart the desired functionality by a variety of active groups/molecules/moieties, depending on the applications. Membrane functionalization can be used to enhance separation capabilities (i.e., affinity, tunable separations) and extend the spectrum of applications towards new areas, such as designing drug delivery systems (by controlled, tunable solute transport), catalysis, or biocatalysis. A large variety of ligands have been used for membrane functionalization, the most common being polymers, amonoacids/polyaminoacids, metal affinity, ion exchange, etc. (8,9). Among these, membrane modification with ion exchange ligands has received extensive attention in a variety of processes and applications including nanofiltration (10,11), enzyme immobilization, and biocatalysis (12,13), catalysis (14,15), and heavy metal capture (16–20). An overview of membrane functionalization techniques and processes is shown in Fig. 1.

Our research group is involved in creating reactive membranes by functionalization with polyligands containing ion exchange groups (i.e., poly(acrylic acid) (PAA)). In particular, our focus is on metal (iron) ion capture and their use in oxidative and reductive reactions for the degradation of toxic organics such as trichloroethylene (TCE), 2,2′-dichlorobiphenyl (DiCB), or pentachlorophenol (PCP). The oxidative pathway, also known as the Fenton reaction, involves the generation of free radicals via the reaction of Fe(II) and H_2O_2. The reductive pathway utilizes metal nanoparticle formation within the membrane domain for catalytic dechlorination of the organic chlorinated compounds. Traditionally, the synthesis of nanoparticles and the application of the Fenton reaction have been performed in the solution phase. However, there are several advantages to immobilizing these metal species within a membrane domain.

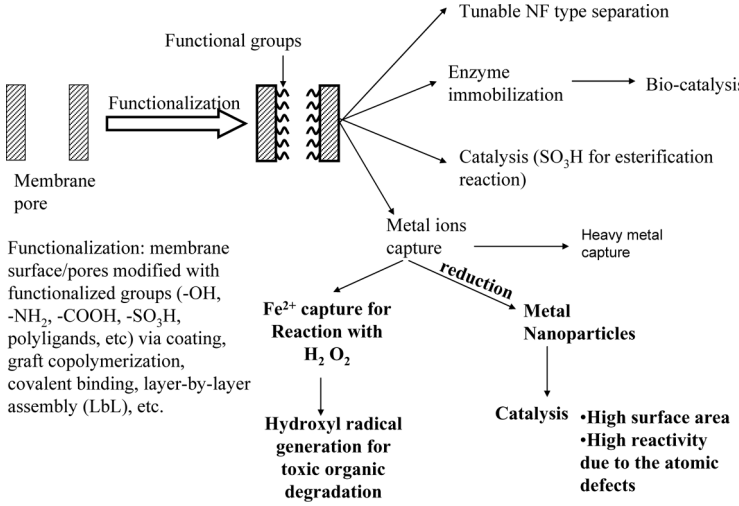

Figure 1. Overview on membrane functionalization and processes.

There are several methods of PAA functionalization on membranes, as shown in Fig. 2. Various membranes can be used as platforms (supports) for PAA functionalization, but should have suitable thermal and chemical stability for the desired application. The simplest method is dipping the membrane in a PAA solution. The PAA diffuses inside the membrane pores and the chains are cross-linked by ethylene glycol (EG) to prevent leaching from the membrane. However, it was shown that PAA is coated primarily on

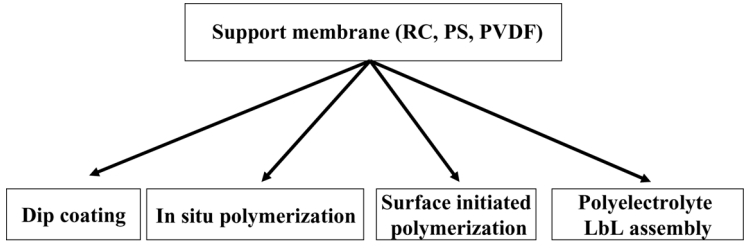

RC – Regenerated cellulose
PS – Polysulfone
PVDF – Polyvinylidene fluoride
LbL – Layer-by-Layer

Figure 2. Various approaches for PAA-functionalization of membrane supports.

the external membrane surface and at the pore mouth, thus blocking the PAA diffusion inside (21). This method does not take advantage of the internal membrane surface, and dramatically reduces the membrane pore size.

Another approach is to polymerize the monomer, acrylic acid, inside the membrane pores. This can be obtained by either surface-initiated or in situ polymerization. In the first case, initiator groups are immobilized on the membrane and the polymerization occurs via a radical transfer mechanism after the addition of the monomer (22). In the second case, the membrane is soaked in polymerization solution containing the initiator, the monomer, and the cross-linking agent. This solution diffuses inside the membrane pores and random polymerization occurs by heating the membrane (23,24).

An additional method of PAA immobilization on membrane supports is by forming polyelectrolyte layer-by-layer (LbL) assemblies via alternating adsorption of polycations and polyanions. Thus, thin films containing oppositely charged polyelectrolytes are formed on the external membrane surface (15,25,26).

Objectives of this research include:

1. Use water-based and solvent-based acrylic acid polymerization (to synthesize PAA) within poly(vinylidene fluoride) (PVDF) membrane pores as platforms for iron capture
2. Synthesize bimetallic nanoparticles within PAA/PVDF membrane created using water-based functionalization
3. Conduct controlled free radical reactions within PAA/PVDF domain
4. Apply membrane-immobilized reductive and oxidative methods for destruction of target species including TCE, DiCB, and PCP

MATERIALS AND METHODS

Materials

All chemicals used were of reagent grade. TCE, ferrous sulfate, sodium citrate, sodium phosphate, hydrogen peroxide (30 wt%), pentane, sodium hydroxide, sulfuric acid, acetonitrile (HPLC-grade), and deionized ultrafiltered (DIUF) water were all purchased from Fisher Scientific. Copper(II) sulfate and potassium persulfate were purchased from EM Science. Toluene, acrylic acid, trimethylolpropane triacrylate (TMPTA), benzoyl peroxide, 3-(2-pyridyl)-5,6-diphenyl-1,2,4,-triazine-4′,4″-disulfonic acid sodium salt (ferrozine), 2,9-dimethyl-1,10-phenanthroline (DMP),

PCP, 1,2-dibromoethane (EDB), and potassium tetrachloropalladate (II) were purchased from Sigma-Aldrich. Chloride reference solution (1000 ppm) was purchased from Thermo Electron Corporation. Sodium nitrate was purchased from LabChem Inc., ethylene glycol was purchased from Mallinckrodt, and naphthalene-d8 and DiCB were purchased from Ultra Scientific. PVDF microfiltration membranes, both hydrophobic (HVHP) and hydrophilic (GVWP), with a thickness of 125 μm and nominal pore sizes of 450 nm and 220 nm, respectively, were obtained from Millipore Corporation.

Methods

Membrane Functionalization

PVDF membranes were coated with PAA by in situ polymerization of acrylic acid. Although various membrane materials can be used for this application, PVDF was chosen for its high chemical and thermal stabilities. The polymerization reaction was carried out in aqueous and organic (toluene) phases. In the organic phase, the polymerization solution containing 70 wt% toluene (solvent), 30 wt% acrylic acid (monomer), 1.2 wt% TMPTA (cross-linker), and 0.5 wt% benzoyl peroxide (initiator) was mixed for 30 min in a closed vessel. The procedure was described in detail previously (23,24).

Aqueous phase in situ polymerization of acrylic acid (green chemistry) was adapted from literature (27,28). The polymerization solution contained 30 wt% acrylic acid (monomer), ethylene glycol (cross-linker, added in a 1:10 molar ratio of EG to acrylic acid), and 1 wt% potassium persulfate (initiator). Each ethylene glycol molecule binds to two –COOH groups thus preventing PAA leaching from the membrane. However, the amount of cross-linking agent has to be kept low in order to maintain free –COOH groups for ion exchange. Under our experimental conditions, about 80% of the –COOH groups are free assuming one molecule of EG binds to two –COOH groups.

For both aqueous-based and solvent-based polymerization, a PVDF membrane was dipped in the polymerization solution for 2 minutes, sandwiched between 2 teflon plates, and placed in an oven at 90°C for 4 hours. Nitrogen gas was continuously supplied to remove oxygen, which acts as an inhibitor for the polymerization reaction. In order to ensure the proper wetting, hydrophobic PVDF membranes were used for solvent-phase polymerization and hydrophilized ones for the aqueous-phase polymerization.

Bimetallic Fe/Pd Nanoparticle Synthesis

The flowchart for membrane functionalization and nanoparticle synthesis is shown in Fig. 3. Prior to Fe^{2+} ion exchange, PAA-coated PVDF membranes were immersed in NaCl (20% wt) solution at pH 10 for 10 hours to convert the –COOH to –COONa form. The purpose was to minimize the pH effects on ion exchange equilibrium, thus enhancing the ion exchange capacity. In the next step, the membrane was washed with DIUF until the pH of the washing solution became neutral. Then, the membrane was immersed in $FeCl_2$ solution (typically 180 mg/L Fe^{2+}) at a pH of 5.5 for 4 hours. Nitrogen gas was bubbled to minimize Fe^{2+} oxidation. The reduction with $NaBH_4$ ensured Fe nanoparticle formation and the membranes were stored in ethanol to prevent oxidation. The secondary metal, Pd, was deposited on the Fe nanoparticles by immersing the membrane in a K_2PdCl_4 solution containing ethanol/water (90:10 vol% mixture), preventing the oxidation of the highly reactive Fe nanoparticles. This created core-shell nanoparticles. The membranes were stored in ethanol until dechlorination reactions were carried out. Batch experiments were performed using either TCE or DiCB in order to determine the reactivity of the immobilized Fe/Pd nanoparticles.

Membrane and Nanoparticle Characterization

SEM-EDS

Surface morphology of the bare, PAA-coated and nanoparticle-modified membranes were examined by Scanning Electron Microscopy instrument, Hitachi S-3200. This instrument was coupled with an X-ray energy dispersive (EDS) apparatus, which was used for membrane elemental analysis.

FTIR

The Fourier Transform Infrared spectra of the bare and PAA-coated PVDF membranes were recorded on a Varian 7000e FTIR with attenuated total reflectance (ATR). Membranes were dried at 90°C for four hours before testing. Data was collected using 128 scans at a resolution of 4 cm^{-1}.

Metal Analysis

Analysis of Pd

Pd containing feed and permeate probes were quantified by Atomic Absorption Spectroscopy (AAS) using a Varian SpectrAA 220 Fast Sequential atomic absorption spectrometer at a wavelength of 246.6 nm. The linear calibration range is between 0.2 and 28 mg/L Pd. The error of analysis was <2%. The material balance was used to determine the amount of Pd deposited as a secondary metal on the membrane.

Analysis of Fe

The amount of Fe captured during ion exchange was quantified using a Varian SpectrAA 220 Fast Sequential atomic absorption spectrometer equipped with a Fisher Scientific Fe data-coded hollow cathode lamp. The lamp was operated at a wavelength of 386.0 nm. The calibration curve was created using 7 different concentrations of Fe ranging from 90 to 900 μmol/L with $R^2 = 0.9993$ and average analytical error of 1.3%.

Analysis of Fe^{2+} Concentration

The concentration of Fe^{2+} was measured using the ferrozine method (29,30). The calibration curve was created using five different concentrations of Fe^{2+} ranging from 9 to 180 μmol/L with $R^2 = 0.992$ and an average analytical error of 3.6%.

Degradation Reactions

Analysis of PCP

The concentration of PCP was measured using a Shimadzu HPLC with photodiode array detector and a Premier C18 5 μm 250 mm × 4.6 mm column. The column was operated under isocratic flow conditions of 0.6 mL/min acetonitrile and 0.2 mL/min water. The calibration curve was created using 9 different quantities of PCP ranging from 0.05 to 2.5 nmol with $R^2 = 0.9998$ and average analytical error of 2.5%.

TCE Analysis by Gas Chromatography

Dechlorination of TCE was conducted by cutting PAA/PVDF membranes containing Fe/Pd nanoparticles (original membranes were of 13.2 cm^2 external area and 125 μm thickness) into small pieces and immersing them in 20 mL sealed vials containing TCE solution. Probes were collected with a syringe at different times. TCE samples were extracted in pentane, and analyzed with a Hewlett Packard Series II 5890 GC-MS. In this analysis, the decrease of TCE concentration in time was monitored and EDB was used as an internal standard. The calibration was performed in between 5 and 120 mg/L TCE, linear $R^2 = 0.9899$, and the average analytical error was <8.5%.

2,2′-Dichlorobiphenyl Analysis by GC-MS

Similar to the previous case, the dechlorination of dichlorobiphenyl was also conducted in 20 mL closed vials and probes being collected at different times. The samples extracted in hexane and analyzed with a Varian CP-3800 GC coupled with a Varian Saturn 2200 MS. The concentrations of the starting compound, DiCB, intermediate—chlorobiphenyl, and final product—biphenyl, were monitored with time.

In the linear range, between 1 and 25 mg/L dichlorobiphenyl, the average analytical error was less than 2%.

RESULTS AND DISCUSSION

PAA/PVDF Functionalized Membrane Characterization

The functionalization of the PVDF membranes with PAA was characterized by FTIR spectroscopy and stimuli-responsive water flux to pH. The chemical structures for the hydrophilized PVDF and PAA-coated PVDF membranes were studied by FTIR-ATR spectroscopy (Fig. 4). The PAA-coated PVDF membrane shows a distinct absorption band at 1710 cm^{-1}, whereas the blank hydrophilic PVDF membrane does not. This band is due to the presence of C=O bond stretching in carboxylic acid groups, indicating successful PAA formation within the functionalized membrane. The strong absorption band at 1140–1280 cm^{-1} is characteristic of CF_2 found in PVDF. Xu and Bhattacharyya (2008) performed both FTIR analysis and STEM-EDS mapping on hydrophobic PVDF membranes functionalized with PAA via the solvent-based method (23). FTIR data showed C=O bond stretching was present in the

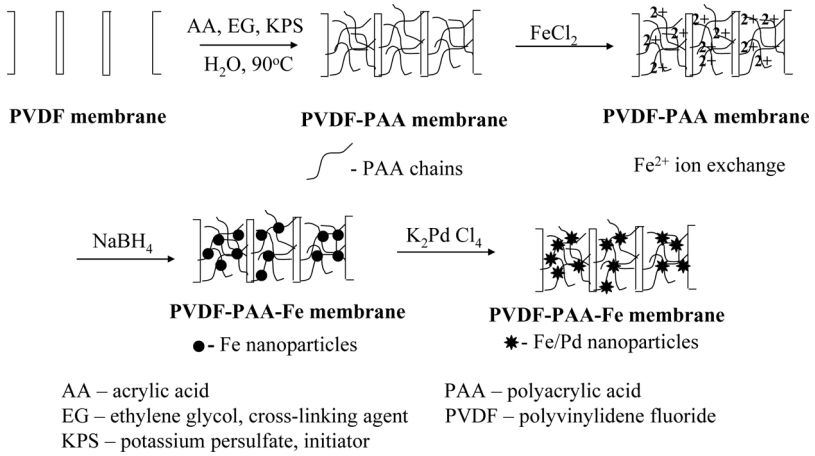

Figure 3. Schematic for PAA coating and Fe/Pd nanoparticle synthesis in PVDF membranes (green chemistry, no solvent use).

modified hydrophobic PVDF membranes, indicating successful PAA functionalization. This bond was not present in the blank hydrophobic PVDF membranes. STEM-EDS mapping indicated the presence of oxygen atoms, also confirming the formation of PAA.

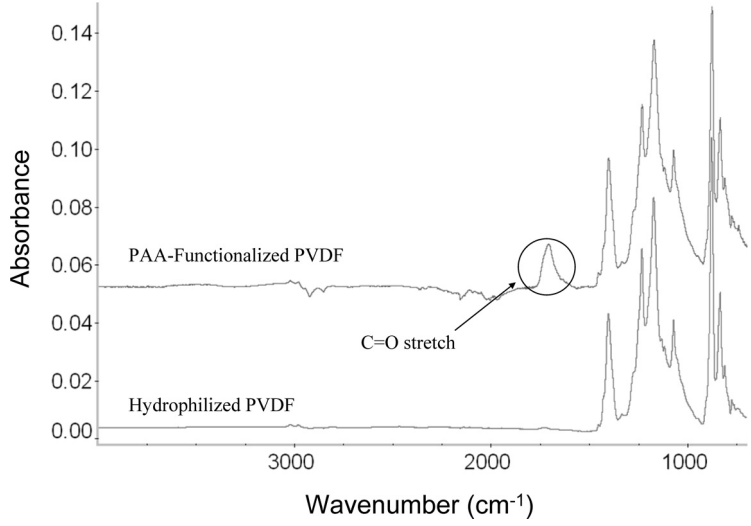

Figure 4. FTIR-ATR spectra for hydrophilized PVDF and PAA-functionalized PVDF membranes.

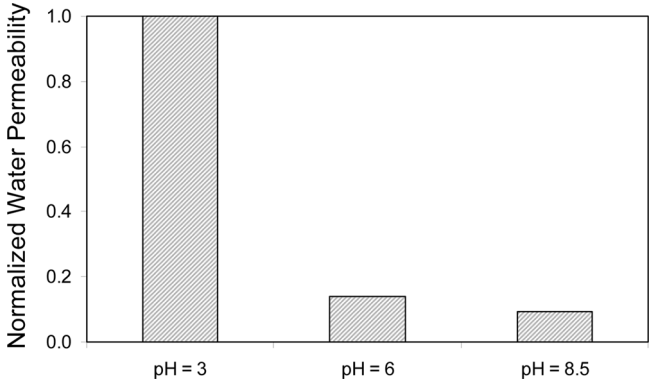

Figure 5. Water permeability dependence on pH for PAA-functionalized PVDF membrane. All flux values are normalized with respect to the permeability at pH = 3 (2.5×10^{-4} cm^3 cm^{-2} bar^{-1} s^{-1}). Pressure ranged between 0.7 and 2.8 bar.

With PAA present within the membrane pores, as indicated by FTIR, one would expect to see a stimuli-responsive water flux to pH. The effect of varying pH on water flux through the PAA/PVDF functionalized membrane is shown in Fig. 5. It can be seen that as the permeate pH is increased, the flux decreases, with a significant drop occurring between pH 3 and pH 6. This is in agreement with the findings of Hu and Dickson (2007), who conducted similar tests on PVDF membrane pores filled with PAA. Since the pK_a of PAA is approximately 4.2, the PAA network will maintain a relatively neutral charge at a low pH, leaving it in a retracted state (13). As the pH is increased, more $-$COOH groups will become ionized, resulting in an elongation of the PAA network due to charge repulsion. While in the elongated state, there is significantly less core leakage and thus lower permeate flux than in the retracted state.

Based on weight gain, the amount of PAA deposited on the various membranes was estimated to be in the range of 3.5 to 4.5 mmol PAA/g dry membrane (4.1 to 4.9 mmol/cm^3 membrane pore volume). Knowing the membrane thickness, the porosity, and the external surface area, the PAA gel occupies 28 to 39% of the membrane pore volume.

Nanoparticle Synthesis and Catalytic Dechlorination

Fe/Pd bimetallic nanoparticles were synthesized within the membrane nanodomain, as described in Section titled ''Membrane and Nanoparticle Characterization.'' SEM imaging was used to examine the surface

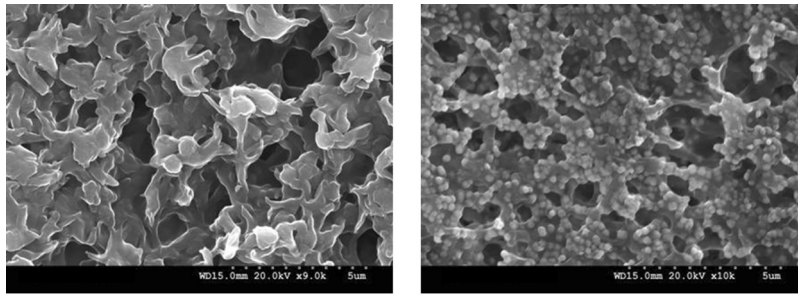

(a) (b)

Figure 6. SEM images for (a) bare PVDF membrane, 9 k (b) PAA-coated PVDF membrane containing immobilized Fe/Pd nanoparticles, 10 k.

morphology for both bare and nanoparticle-modified PVDF membranes (Figs. 6a and b). The presence of spherical grains clearly indicates nanoparticle formation on the membrane surface. Higher resolution (100 k) imaging shows that there is a greater tendency for the particle agglomeration on the membrane surface (Fig. 7a), and the base particle size was estimated to be about 50 nm. Inside the membrane (Fig. 7b), there are more discreet particles with an approximate diameter of 50 nm. This reduced agglomeration as compared to the external surface is due to the fact that the chains are cross-linked and their mobility is reduced. The particle size can be modulated by changing the degree of cross-linking. At lower degrees of cross-linking, the particle size is expected to be higher since there is more chain mobility and adjacent nanoparticles can agglomerate, forming larger particles. For catalytic

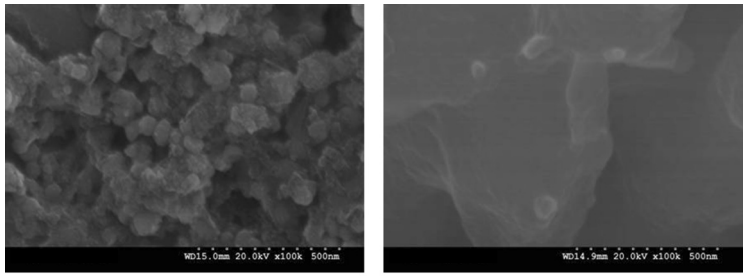

(a) (b)

Figure 7. SEM images (100 k) for PAA-coated PVDF membranes containing immobilized Fe/Pd nanoparticles (a) External surface (b) Cross-section through the membrane thickness.

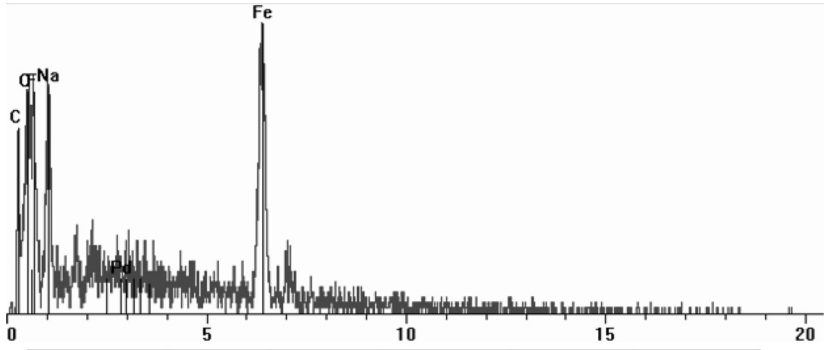

Element	Line	keV	KRatio	Wt%	At%
O	KA1	0.523	0.0634	18.46	20.16
C	KA1	0.277	0.0704	33.79	49.15
F	KA1	0.677	0.0424	16.08	14.79
Na	KA1	1.041	0.0302	13.79	10.47
Fe	KA1	6.403	0.1457	16.80	5.25
Pd	LA1	2.838	0.0086	1.08	0.18
Total			**0.3606**	**100.00**	**100.00**

Fe:Na:O = 3.8:1.9:1
Ideally, **Fe:Na:O = 4:2:1**

Figure 8. EDX spectrum of bimetallic Fe/Pd nanoparticles embedded in PAA-coated PVDF membrane.

applications, smaller particles are preferred as they ensure a higher surface area and more accessibility to the active sites.

Elemental analysis of the modified membrane was performed by EDS (Fig. 8). From ion exchange principles, theoretically 1 mol of Fe^{2+} binds to two –COOH groups, yielding an Fe:O molar ration of 1:4. After reduction with $NaBH_4$, Fe is replaced with Na^+, resulting in 1 mol Na^+ per –COOH group, yielding a Na:O molar ratio of 1:2. The results from EDS (Fe:Na:O molar ratio of 3.8:1.9:1) are close to the theoretical values (Fe:Na:O molar ratio of 4:2:1) showing that there is no physical metal adsorption on the membrane, only ion exchange.

As mentioned earlier, Fe/Pd-modified membranes were tested for dechlorination of two target toxic organic compounds: TCE and DiCB. The dechlorination results for the two toxic compounds performed with different membranes are shown in Figs. 9 and 10, respectively. The metal

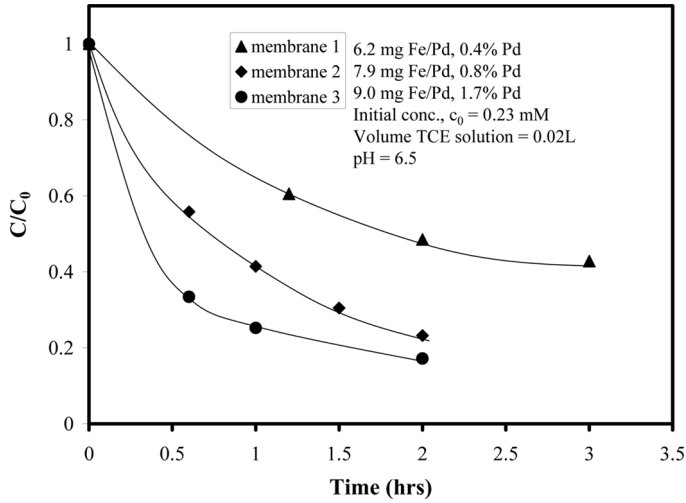

Figure 9. TCE dechlorination for three PAA/PVDF – Fe/Pd membranes (13.2 cm^2 external area, 125 μm thickness). Control experiment conducted with PAA/PVDF membrane (no nanoparticles) showed negligible TCE loss.

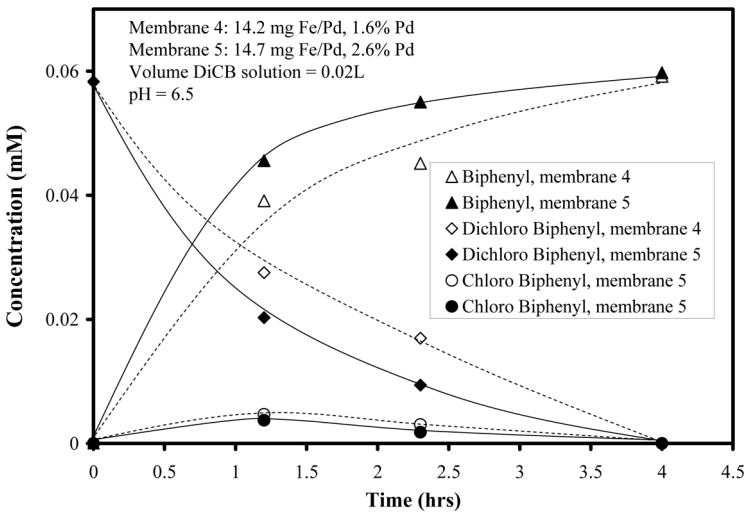

Figure 10. The dechlorination of dichlorobiphenyl (DiCB) with two PAA/PVDF – Fe/Pd membranes (13.2 cm^2 external area, 125 μm thickness). Control experiment conducted with PAA/PVDF membrane (no nanoparticles) indicated no DiCB loss.

Table 1. Metal loading on various PAA-coated PVDF membranes and surface-area-normalized reaction rate constants for dechlorination

Membrane	Chlorinated compound	Fe (mg)	%wt Pd (compared to Fe)	k_{SA} (L/m^2h)	r^2
1	TCE	6.2	0.4	0.059	0.937
2	TCE	7.9	0.8	0.069	0.982
3	TCE	9.0	1.7	0.114	0.974
4	DiCB	14.2	1.6	0.052	0.989
5	DiCB	14.7	2.6	0.070	0.996

TCE–Trichloroethylene.
DiCB–2,2′-Dichlorobiphenyl.

loading characteristics for the five membranes used in dechlorination studies are shown in Table 1.

The data in Figs. 9 and 10 was fitted assuming a pseudo-first order rate law, and from a $\ln(C/C_0)$ vs time plot, k_{obs}, the observed pseudo-first order constant was determined. The surface-area-normalized rate constant, k_{SA} (L/m^2h), can be calculated from these k_{obs} values using Eq. 1 where C_0 is the initial concentration of the chlorinated compound, C is the concentration of the chlorinated compound at time t (h), a_S is the specific surface area of the nanoparticles (m^2/g), and ρ_m is the nanoparticle loading (g/L).

$$dC/dt = k_{obs}C = k_{SA}a_S\rho_m C \quad (1)$$

Assuming discreet spherical particles with a diameter of 50 nm, as observed from SEM imaging, a_S was calculated to be $15\,m^2/g$. The nanoparticle loading was determined by dividing the amount of metal loaded on the membrane by the volume of the chlorinated solution (0.02 L). Based on these assumptions, the k_{SA} value for each system was calculated, as shown in Table 1.

In a Fe/Pd bimetallic system, the role of Fe (reactant) in zero-valent form is to generate hydrogen via a corrosion reaction. Pd acts as a hydrogenation catalyst and thus can be considered as the active sites in the bimetallic system. From the data in Table 1, it can be observed that k_{SA} value increases with the amount of Pd in bimetallic particles. Pd surface coverage can be estimated based on 50 nm particle size and Pd cross-sectional area of $0.0787\,nm^2$ (31). For the five membranes used in the dechlorination experiments, Pd coverage was estimated to be in the range between 0.10 monolayers at the lowest Pd loading and 0.75 monolayers at the highest Pd loading. Since Pd coverage is less than

1 monolayer for all membranes, all Pd atoms are considered active sites, indicating the k_{SA} value increases with increasing Pd loading. It is interesting to observe that the k_{SA} value for membrane #5 (14.7 mg Fe/Pd, 2.6% wt Pd) is very similar (within 10%) to the one previously reported (24) under similar conditions (15 mg Fe loading, 2.3%wt Pd). For that case, the matrix for Fe/Pd nanoparticle formation was prepared using a different methodology, solvent-based acrylic acid polymerization.

Membrane-Immobilized Free Radical Reactions

Free Radical Reactions

Advanced oxidative techniques are commonly used for organic contaminant degradation. This includes the use of electrochemical, photolytic, and other free radical generating techniques (32). The generation of hydroxyl radicals via the reaction of ferrous iron and hydrogen peroxide was first proposed by Haber and Weiss in 1934 (Eq. 2) (33,34).

$$Fe^{2+} + H_2O_2 \rightarrow Fe^{3+} + OH^- + OH\bullet \qquad k_2 = 63\,M^{-1}s^{-1} \qquad (2)$$

Hydroxyl radicals are powerful oxidants which are highly unselective and capable of oxidizing both aliphatic and aromatic compounds (35). This reaction is autocatalytic and continues to propagate via Eqs. 3–7 until all hydrogen peroxide has been consumed (33,36,37).

$$Fe^{3+} + H_2O_2 \rightarrow Fe^{2+} + HO_2\bullet + H^+ \qquad k_3 = 2 \times 10^{-3}M^{-1}s^{-1} \qquad (3)$$

$$Fe^{2+} + OH\bullet \rightarrow Fe^{3+} + OH^- \qquad k_4 = 3.2 \times 10^{8}M^{-1}s^{-1} \qquad (4)$$

$$Fe^{3+} + HO_2\bullet \rightarrow Fe^{2+} + O_2 + H^+ \qquad k_5 = 2 \times 10^{3}M^{-1}s^{-1} \qquad (5)$$

$$H_2O_2 + OH\bullet \rightarrow H_2O + HO_2\bullet \qquad k_6 = 3.3 \times 10^{7}M^{-1}s^{-1} \qquad (6)$$

$$OH\bullet + OH\bullet \rightarrow H_2O_2 \qquad k_7 = 6 \times 10^{9}M^{-1}s^{-1} \qquad (7)$$

The Fenton reaction is most efficient at a low pH, where the consumption of available Fe^{2+} is very rapid. The reduction of Fe^{3+} is much slower than the oxidation of Fe^{2+} and therefore becomes the rate-limiting step in the catalytic cycle once most of the Fe^{2+} has been converted to Fe^{3+}. Several investigators have opted to use Fe(III) to initialize the decomposition of hydrogen peroxide instead of Fe(II) in order to promote the generation of other radical species ($HO_2\bullet$ and $O_2\bullet^-$)

for use in degrading contaminants that are less susceptible to attack by OH• (38).

The Fenton reaction is much less efficient at near-neutral pH: in aerobic environments, Fe(II) is rapidly oxidized to Fe(III) which precipitates as $Fe(OH)_3$, preventing its reduction to Fe(II), thus terminating the catalytic cycle. Much work has been done towards modifying the Fenton reaction so as to avoid these problems through the addition of a chelating agent (39,40). A chelate present in solution binds with the iron species, greatly reducing the rate of Fe(II) oxidation and eliminating the precipitation of Fe(III) as $Fe(OH)_3$ at near-neutral pH. The advantages of iron chelation in the aqueous phase can be applied to the membrane domain via the incorporation of ion exchange groups.

Significant quantities of hydrogen peroxide are needed for practical applications, requiring the dilution of concentrated solutions; however, highly concentrated hydrogen peroxide can be hazardous to transport. Our group has developed a technique for the enzymatic production of hydrogen peroxide within the membrane domain (12,13,41). Glucose oxidase (GOX) is a well-known and robust enzyme which catalyzes the reaction of glucose and O_2 to form hydrogen peroxide and gluconic acid at room temperature. GOX was electrostatically immobilized in a LbL assembly and glucose solution was passed through the membrane. Kinetic studies indicated there was minimal reduction in GOX activity ($10 \pm 5\%$) due to immobilization (13). Such a platform could be easily implemented for on-site hydrogen peroxide generation therefore avoiding the need to transport of concentrated solutions.

Membrane-Immobilized Fenton Reaction in PAA/PVDF Membrane

Ion exchange groups immobilized within membrane pores have been used for a variety of applications involving metal capture. Several investigators have utilized Nafion membranes for the immobilization of Fe(II)/Fe(III) and subsequent reaction with H_2O_2. Espro et al. (2000, 2001) (42,43) applied an Fe(II)-H_2O_2 Fenton system at elevated temperature and pressure for the oxidation of light alkanes. Fernandez et al. (2003) used a photoassisted Fe(III)-H_2O_2 system for the oxidation of target organics (44). Parra et al. (2004). utilized a similar photoassisted Fenton reaction for the oxidation of 4-chlorophenol (45).

The relative amounts of Fe(II) and Fe(III) present within the membrane domain determine the rate at which H_2O_2 is decomposed. The conversion of Fe(II) to Fe(III) within the PAA-filled pores was investigated by passing a solution containing 150 μmol/L H_2O_2 through the membrane via convection. As the H_2O_2 permeated, Fe(II) was gradually

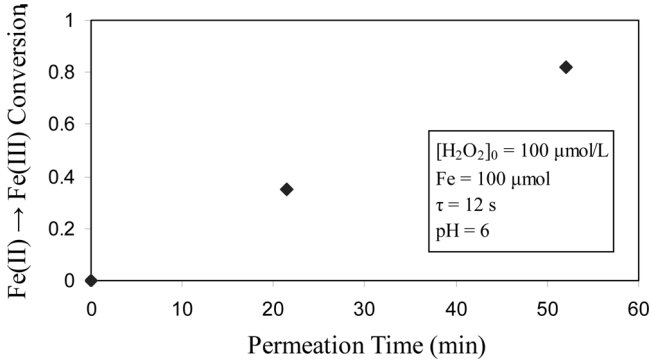

Figure 11. Fe(II) → Fe(III) conversion for membrane-immobilized Fenton reaction as a function of permeation time for feed containing 100 μmol/L H_2O_2. $\Delta P = 0.68$ bar. External membrane area $= 33.2\,cm^2$, thickness $= 125\,\mu m$.

converted to Fe(III), until only Fe(III) remained, as seen in Fig. 11. No iron was released during H_2O_2 permeation. It is important to note that in solutions at pH = 6, soluble Fe(III) is not present as Fe^{3+}, but mainly as $Fe(OH)_2^+$ and $Fe(OH)_{3,aq}$. Because of this, COO-Fe(III) complexes may also be hydroxylated within the PAA domain. Until all iron is present as Fe(III), the rate of H_2O_2 decomposition will not reach a steady state since the apparent concentrations of the iron species are constantly changing. This is because the reaction of Fe(III) with H_2O_2 and/or radical species becomes the rate-limiting step.

For steady state experimentation, Fe(III) was not directly loaded into the membrane since it would precipitate at the pH required to obtain significant loading (above the pK_a of PAA). Therefore, 22 μmol of Fe(II) were loaded into the membrane (external area $= 33.2\,cm^2$, thickness $=$ 125 μm) and oxidized with a solution containing H_2O_2 until complete conversion to Fe(III) was achieved. Hydrogen peroxide solutions at varying concentrations and residence times were then permeated through the membrane. Figure 12 shows the conversion of H_2O_2 as a function of residence time at pH = 6. Residence time was varied by changing ΔP. Assuming the membrane behaved as a continuous stirred-tank reactor and the decomposition of H_2O_2 was first-order, the first-order rate constant, k_{CSTR}, was calculated to be $(7.8 \pm 0.8) \times 10^{-3}\,s^{-1}$ (shown in Fig. 12) using Eq. 8, where $[H_2O_2]_0$ is the feed concentration of H_2O_2, $[H_2O_2]$ is the permeate concentration of H_2O_2, τ is the residence time, and r_{H2O2} is the rate of H_2O_2 decomposition. Assuming [Fe(III)] is constant, the second-order rate constant, k'_{CSTR} was found to be $(8.1 \pm 0.7) \times 10^{-2}\,M^{-1}s^{-1}$ (Eq. 9).

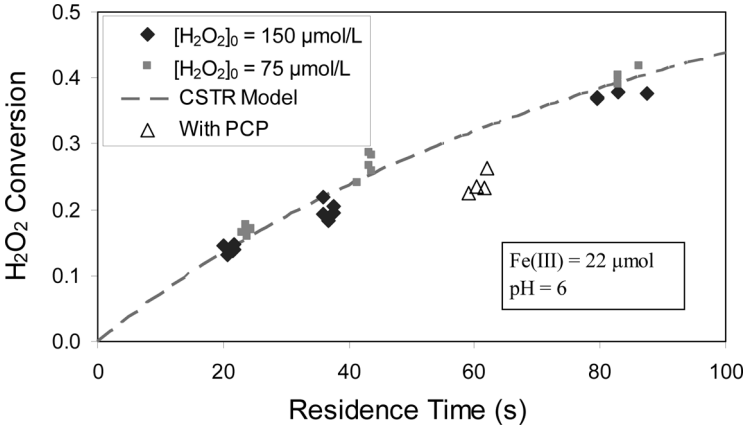

Figure 12. H_2O_2 conversion as a function of residence time for membrane-immobilized Fenton reaction with 22 µmol of captured Fe(III) at pH = 6. $[H_2O_2]_0 = 150$ µmol/L for feed with 20 µmol/L PCP. Residence time was varied by changing ΔP. External membrane area = 33.2 cm^2, thickness = 125 µm.

$$-r_{H_2O_2} = \frac{[H_2O_2]_0 - [H_2O_2]}{\tau} = k_{CSTR} \times [H_2O_2] \quad (8)$$

$$k_{CSTR} = k'_{CSTR} \times [Fe(III)] \quad (9)$$

The calculated value is approximately 40 times greater than k_3. This is in agreement with the investigations of (46), who found the rate of azo-dye degradation in a photo-assisted Fenton reaction immobilized in a Nafion membrane was similar to that of a homogeneous reaction with approximately 100 times more Fe^{3+}. It has been reported that Fe-carboxylate complexes on the surface of the membrane could be responsible for this reactivity (44). These complexes may also be responsible for the stability of PAA in the presence of free radicals (44).

PCP Degradation

Pentachlorophenol (PCP) was once a widely used fungicide for wood preservation that was banned from use in 1987. It is a toxic compound that can still be found in soils at several sites of wood preserving industries. PCP degradation via reaction with free radicals has been conducted, but most studies have been performed either with the assistance of UV light (photo-Fenton) (47,48) or at high temperature (49). Liou et al. used

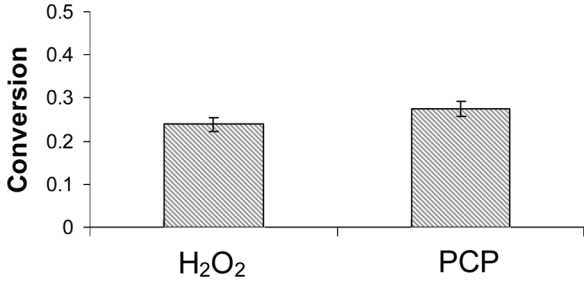

Figure 13. H_2O_2 and PCP conversion for membrane-immobilized Fenton reaction with 22 μmol of captured Fe(III) at pH = 6. Feed containes 150 μmol/L H_2O_2 and 20 μmol/L PCP. $\tau = 60 \pm 2$ s, water permeability = 1.7×10^{-4} cm^3 cm^{-2} bar^{-1} s^{-1}. External membrane area = 33.2 cm^2, thickness = 125 μm.

a Fe^{3+}-resin system to oxidize PCP in solution at elevated temperatures, achieving over 90% degradation. Fukushima and Tatsumi (2001) achieved greater than 90% removal of PCP after 300 min of UV-irradiation in a H_2O_2/Fe(III)/humic acid system (47).

By permeating a solution containing 150 μmol/L H_2O_2 and 20 μmol/L PCP through a PAA/PVDF membrane containing immobilized Fe(III), PCP was degraded at initial pH = 6 and 25°C temperature (Fig. 13). The conversions of H_2O_2 and PCP were 24% ± 2% and 27% ± 2% (5.4 μmol/L), respectively, for a residence time of 60 ± 2 s. This corresponded to 7.1 mol H_2O_2 consumed/mol PCP degraded. These conversions can be adjusted by varying the amount of iron loading, residence time, and/or the pH. This degradation of PCP is greater than the ~5% (~2.5 μmol/L) results previously reported by (50) using solution-phase Fe(III)-H_2O_2 reactions (with higher H_2O_2 concentration) at pH = 5.

H_2O_2 conversion for the solutions containing PCP was lower than those containing no PCP, as seen in Fig. 12. This is to be expected since PCP acts as a scavenger of hydroxyl radicals, lowering the rate of Equation 6 and therefore the rate of H_2O_2 decomposition.

CONCLUSIONS

Functionalization of PVDF membranes with PAA was achieved using water and solvent-based acrylic acid polymerization methods. These membranes were stimuli-responsive, the flux through which was successfully controlled by varying the pH of the feed. The negatively charged ion exchange groups within the membrane pores were used to capture ferrous

iron. These membranes were then employed to degrade target compounds using reductive and oxidative strategies. For the reductive approach, the immobilized Fe^{2+} was reduced to Fe^0 and subsequently doped with Pd. This resulted in the formation of bimetallic (Fe/Pd) nanoparticles with an average size of 50 nm inside of the membrane pores. Particle aggregation was present only on the membrane surface and not within the membrane pores. The dependence of Fe/Pd-modified membrane reactivity created using water-based acrylic acid polymerization on Pd loading was established for the dechlorination of two model compounds, TCE and DiCB. Complete dechlorination of DiCB was obtained within 4 h. The surface-area-normalized rate constant for reaction with dichlorobiphenyl was within 10% of the values previously reported using solvent-based methods for PAA/PVDF functionalization. For the oxidative approach, the conversion of Fe(II) to Fe(III) within the PAA/PVDF domain was quantified. The observed rate constant for H_2O_2 degradation via reaction with immobilized Fe(III) as a function of residence time through the membrane was calculated from experimental data. The subsequent generation of hydroxyl radicals in the same system indicated a successful degradation of pentachlorophenol (PCP).

ACKNOWLEDGEMENTS

This research was supported by the NIEHS/SBRP (Grant number: P42ES007380) and NSF-IGERT programs. Alex Montague was supported by the NSF/REU program.

REFERENCES

1. Ho, W.; Sirkar, K.K. (1992) *Membrane Handbook*; Chapman and Hall: New York.
2. Stamatialis, D.F.; Papenburg, B.J.; Girones, M.; Saiful, S.; Bettahalli, S.N.M.; Schmitmeier, S.; Matthias, W. (2008) Medical applications of membranes: Drug delivery, artificial organs and tissue engineering. *Journal of Membrane Science*, *308* (1–2): 1–34.
3. Fritzmann, C.; Lowenberg, J.; Wintgens, T.; Melin, T. (2007) State-of-the-art of reverse osmosis desalination. *Desalination*, *216* (1–3): 1–76.
4. Charcosset, C. (2006) Membrane processes in biotechnology: An overview. *Biotechnology Advances*, *24* (5): 482–492.
5. Noble, R.D.; Stern, S.A. (1995) Membrane Separations Technology: Principles and Applications; Elsevier Science Ltds.
6. Bhattacharyya, D.; Butterfield, D.A. (2003) *New Insights into Membrane Science and Technology: Polymeric and Biofunctional Membranes*; Elsevier, Amsterdam.

7. Ng, A.N.L.; Kim, A.S. (2007) A mini-review of modeling studies on membrane bioreactor (MBR) treatment for municipal wastewaters. *Desalination*, *212* (1–3): 261–281.
8. Klein, E. (2000) Affinity membranes: A 10-year review. *Journal of Membrane Science*, *179* (1–2): 1–27.
9. Shi, W.; Shen, Y.; Ge, D.; Xue, M.; Cao, H.; Huang, S.; Wang, J.; Zhang, G.; Zhang, F. (2008) Functionalized anodic aluminum oxide (AAO) membranes for affinity protein separation. *Journal of Membrane Science*, *325* (2): 801–808.
10. Hollman, A.M.; Bhattacharyya, D. (2004) Pore-assembled multilayers of charged polypeptides in microporous membranes for ion separation. *Langmuir*, *20* (13): 5418–5424.
11. Hu, K.; Dickson, J.M. (2007) Development and characterization of poly(vinylidene fluoride)-poly(acrylic acid) pore-filled pH-sensitive membranes. *Journal of Membrane Science*, *301* (1–2): 19–28.
12. Smuleac, V.; Butterfield, D.A.; Bhattacharyya, D. (2006) Layer-by-layer-assembled microfiltration membranes for biomolecule immobilization and enzymatic catalysis. *Langmuir*, *22* (24): 10118–10124.
13. Datta, S.; Cecil, C.; Bhattacharyya, D. (2008) Functionalized membranes by layer-by-layer assembly of polyelectrolytes and in situ polymerization of acrylic acid for applications in enzymatic catalysis. *Industrial & Engineering Chemistry Research*, *47* (14): 4586–4597.
14. Shah, T.N.; Goodwin, J.C.; Ritchie, S.M.C. (2005) Development and characterization of a microfiltration membrane catalyst containing sulfonated polystyrene grafts. *Journal of Membrane Science*, *251* (1–2): 81–89.
15. Kidambi, S.; Bruening, M.L. (2005) Multilayered polyelectrolyte films containing palladium nanoparticles: synthesis, characterization, and application in selective hydrogenation. *Journal of Materials Chemistry*, *17* (2): 301–307.
16. Hestekin, J.A.; Bachas, L.G.; Bhattacharyya, D. (2001) Poly(amino acid)-functionalized cellulosic membranes: Metal sorption mechanisms and results. *Industrial & Engineering Chemistry Research*, *40* (12): 2668–2678.
17. Ritchie, S.M.C.; Bachas, L.G.; Olin, T.; Sikdar, S.K.; Bhattacharyya, D. (1999) Surface modification of silica- and cellulose-based microfiltration membranes with functional polyamino acids for heavy metal sorption. *Langmuir*, *15* (19): 6346–6357.
18. Vasudevan, T.; Das, S.; Sodaye, S.; Pandey, A.K.; Reddy, A.V.R. (2009) Pore-functionalized polymer membranes for preconcentration of heavy metal ions. *Talanta*, *78* (1): 171–177.
19. Ladhe, A.R.; Frailie, P.; Hua, D.; Darsillo, M.; Bhattacharyya, D. (2009) Thiol-functionalized silica–mixed matrix membranes for silver capture from aqueous solutions: Experimental results and modeling. *Journal of Membrane Science*, *326* (2): 460–471.
20. Sgarlata, C.; Arena, G.; Longo, E.; Zhang, D.; Yang, Y.; Bartsch, R.A. (2008) Heavy metal separation with polymer inclusion membranes. *Journal of Membrane Science*, *323* (2): 444–451.

21. Xu, J.; Dozier, A.; Bhattacharyya, D. (2005) Synthesis of nanoscale bimetallic particles in polyelectrolyte membrane matrix for reductive transformation of halogenated organic compounds. *Journal of Nanoparticle Research*, *7* (4–5): 449–467.
22. Singh, N.; Wang, J.; Ulbricht, M.; Wickramasinghe, S.R.; Husson, S.M. (2008) Surface initiated atom transfer radical polymerization: a new method for preparation of polymeric membrane adsorbers. *Journal of Membrane Science*, *309* (1–2): 64–72.
23. Xu, J.; Bhattacharyya, D. (2008) Modeling of Fe/Pd nanoparticle-based functionalized membrane reactor for PCB dechlorination at room temperature. *Journal of Physical Chemistry C*, *112* (25): 9133–9144.
24. Xu, J.; Bhattacharyya, D. (2007) Fe/Pd nanoparticle immobilization in microfiltration membrane pores: Synthesis, characterization, and application in the dechlorination of polychlorinated biphenyls. *Industrial & Engineering Chemistry Research*, *46* (8): 2348–2359.
25. Dai, J.; Bruening, M.L. (2002) Catalytic nanoparticles formed by reduction of metal ions in multilayered polyelectrolyte films. *NanoLetters*, *2* (5): 497–501.
26. Dotzauer, D.M.; Dai, J.; Sun, L.; Bruening, M.L. (2006) Catalytic membranes prepared using layer-by-layer adsorption of polyelectrolyte/metal nanoparticle films in porous supports. *NanoLetters*, *6* (10): 2268–2272.
27. Dayal, U.; Mehta, S.K.; Choudhary, M.S.; Jain, R.C. (1999) Synthesis of acrylic super absorbents. *Polymer Reviews*, *39* (3): 507–525.
28. Jiang, L.; Gao, Q.; Yu, Y.; Wu, D.; Wu, Z.; Wang, W.; Yang, W.; Jin, R. (2007) Synthesis and characterization of stimuli-responsive poly(acrylic acid) grafted silica nanoparticles. *Smart Materials and Structures*, *16* (6): 2169–2174.
29. Voelker, B.M.; Sulzberger, B. (1996) Effects of fulvic acid on Fe(II) oxidation by hydrogen peroxide. *Environmental Science & Technology*, *30* (4): 1106–1114.
30. Stookey, L.L. (1970) Ferrozine – A new spectrophotometric reagent for iron. *Analytical Chemistry*, *42* (7): 779–781.
31. Nutt, M.; Hughes, J.B.; Wong, M. (2005) Designing Pd-on-Au bimetallic nanoparticle catalysts for trichloroethylene hydrodechlorination. *Environmental Science & Technology*, *39* (5): 1346–1353.
32. Laine, D.F.; Cheng, I.F. (2007) The destruction of organic pollutants under mild conditions: A review. Microchemical Journal, *85* (2): 183–193.
33. Haber, F.; Weiss, J. (1934) The catalytic decomposition of hydrogern peroxide by iron salts. Proceedings of the Royal Society of London. Series A, Mathematical and Physical Sciences, *A147* (861): 332–351.
34. De Laat, J.; Gallard, H. (1999) Catalytic decomposition of hydrogen peroxide by Fe(III) in homogeneous aqueous solution: Mechanism and kinetic modeling. *Environmental Science & Technology*, *33* (16): 2726–2732.
35. Watts, R.J.; Teel, A.L. (2006a) Treatment of Contaminated Soils and Groundwater Using ISCO. Practice Periodical of Hazardous, Toxic, and Radioactive Waste Management, *10* (1): 2–9.
36. Lin, S.S.; Gurol, M.D. (1998) Catalytic decomposition of hydrogen peroxide to iron oxide: kinetics, mechanism, and implications. *Environmental Science & Technology*, *32* (10): 1417–1423.

37. Pignatello, J.J.; Oliveros, E.; MacKay, A. (2006) Advanced oxidation processes for organic contaminant destruction based on the Fenton reaction and related chemistry. *Critical Reviews in Environmental Science and Technology*, *36* (1): 1–84.
38. Watts, R.J.; Teel, A.L. (2006b) Mechanism for the destruction of carbon tetrachloride and chloroform DNAPLs by modified Fenton's reagent. *Journal of Contaminant Hydrology*, *85* (3–4): 229–246.
39. Li, Y.; Bachas, L.G.; Bhattacharyya, D. (2005) Kinetic studies of trichlorophenol destruction by chelate-based Fenton reaction. *Environmental Engineering Science*, *22* (6): 756–771.
40. Seol, Y.; Javandel, I. (2008) Citric acid-modified Fenton's reaction for the oxidation of chlorinated ethylenes in soil solution systems. *Chemosphere*, *72* (4): 537–542.
41. Ahuja, D.K.; Bachas, L.G.; Bhattacharyya, D. (2007) Modified Fenton reaction for trichlorophenol dechlorination by enzymatically generated H_2O_2 and gluconic acid chelate. *Chemosphere*, *66* (11): 2193–2200.
42. Espro, C.; Frusteri, F.; Arena, F.; Parmaliana, A. (2000) Selective oxidation of propane on a Nafion-based catalytic membrane mediated by Fe(II)–H_2O_2 Fenton system. *Journal of Molecular Catalysis A: Chemical*, *159* (2): 359–364.
43. Espro, C.; Arena, F.; Frusteri, F.; Parmaliana, A. (2001) On the potential of the multifunctional three phase catalytic membrane reactor in the selective oxidation of light alkanes by Fe^{2+}–H_2O_2 Fenton system. *Catalysis Today*, *67* (1–3): 247–256.
44. Fernandez, J.; Nadtochenko, V.; Enea, O.; Bozzi, A.; Yuranova, T.; Kiwi, J. (2003) Testing and performance of immobilized Fenton photoreactions via membranes, mats, and modified copolymers. *International Journal of Photoenergy*, *5* (2): 107–113.
45. Parra, S.; Henao, L.; Mielczarski, E.; Mielczarski, J.; Albers, P.; Suvorova, E.; Guindet, J.; Kiwi, J. (2004) Synthesis, testing, and characterization of a novel Nafion membrane with superior performance in photoassisted immobilized Fenton catalysis. *Langmuir*, *20* (13): 5621–5629.
46. Fernandez, J.; Bandara, J.; Lopez, A.; Albers, P.; Kiwi, J. (1998) Efficient photo-assisted Fenton catalysis mediated by Fe ions on Nafion membranes active in the abatement of non-biodegradable azo-dye. *Chemical Communciations*, (14): 1493–1494.
47. Fukushima, M.; Tatsumi, K. (2001) Degradation pathways of pentachlorophenol by photo-Fenton systems in the presence of iron(III), humic acid, and hydrogen peroxide. *Environmental Science & Technology*, *35* (9): 1771–1778.
48. Engwall, M.A.; Pignatello, J.J.; Grasso, D. (1999) Degradation and detoxification of the wood preservatives creosote and pentachlorophenol in water by the photofenton reaction. *Water Research*, *33* (5): 1151–1158.
49. Liou, R.-M.; Chen, S.-H.; Hung, M.-Y.; Hsu, C.-S. (2004) Catalytic oxidation of pentachlorophenol in contaminated soil suspensions by Fe^{+3}-resin/H_2O_2. *Chemosphere*, *55* (9): 1271–1280.